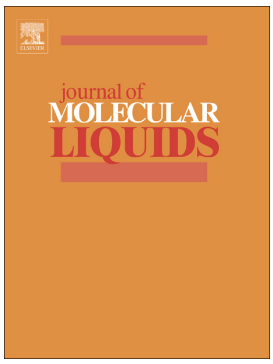

Intermolecular forces in 1-butyl-3-methylimidazolium bis(trifluoromethylsulfonyl)imide + ethanol mixtures

Rafael Alcalde, Mert Atilhan, Santiago Aparicio

PII: S0167-7322(17)36058-0
DOI: doi:10.1016/j.molliq.2018.02.064
Reference: MOLLIQ 8706

To appear in: *Journal of Molecular Liquids*

Received date: 18 December 2017
Revised date: 12 February 2018
Accepted date: 14 February 2018

Please cite this article as: Rafael Alcalde, Mert Atilhan, Santiago Aparicio , Intermolecular forces in 1-butyl-3-methylimidazolium bis(trifluoromethylsulfonyl)imide + ethanol mixtures. The address for the corresponding author was captured as affiliation for all authors. Please check if appropriate. Molliq(2017), doi:10.1016/j.molliq.2018.02.064

Intermolecular Forces in 1-Butyl-3-methylimidazolium Bis(trifluoromethylsulfonyl)imide + Ethanol Mixtures

Rafael Alcalde,[a] Mert Atilhan[*b,c] and Santiago Aparicio[*a]

[a] Department of Chemistry, University of Burgos, 09001 Burgos, Spain

[b] Department of Chemical Engineering, Texas A&M University at Qatar, Doha, Qatar

[c] Gas and Fuels Research Center, Texas A&M University, College Station, TX, USA

[*]Corresponding author: sapar@ubu.es (S.A.) and mert.atilhan@tamu.edu (M.A.)

ABSTRACT: The characteristics of intermolecular forces in 1-butyl-3-methylimidazolium Bis(trifluoromethylsulfonyl)imide + ethanol mixtures were studied in the full composition range using a combined experimental and theoretical approach. Molecular clusters were used to model the short-range interactions between the ionic liquid and the primary alcohol, studied using density functional theory calculations, inferring preferred interaction sites, strength of interactions and topological characteristics of intermolecular forces. Dynamic viscosity and refraction index were measured as a function of mixture composition and temperature and analysed in terms of evolution of intermolecular forces. Raman IR studies were carried out and the analysis of selected spectral regions allowed to characterize hydrogen bonding evolution for all the possible interacting sites.

Highlights

- Imidazolium ionic liquids.
- Mixtures.
- Experimental and theoretical study.
- Intermolecular forces.
- Hydrogen bonding.

KEYWORDS: ionic liquid, imidazolium, molecular solvent, mixtures, DFT, Raman, hydrogen bonding.

1. Introduction

Mixtures of Ionic liquids (ILs) + molecular solvents (MSs) have attracted attention in the literature [1,2,3,4,5,6,7], the main purpose of these studies was to analyse the evolution of intermolecular forces upon mixing [8,9,10] and its relationship with macroscopic thermophysical properties, and thus, for fine tuning the ILs properties [11,12,13]. The development of ILs+OSs mixtures is a suitable approach for controlling ion-ion intermolecular forces, fine tuning the physicochemical properties of the mixed solvents according to the needs for the considered technological applications. Likewise, ILs+OSs mixtures allows one to overcome some of the unsuitable properties of ILs, such as high viscosity, which can be modulated through the mixtures' concentration [14,15,16]. MacFarlane et al. [17] have recently proposed ILs+MSs mixtures as the fourth evolution in ILs technologies because of the appearance of physical phenomena not present in pure ILs and the possibilities of developing new technologies. Regarding the physicochemical behaviour of ILs+MSs mixtures, it should be remarked that they are different from common electrolyte solutions because often they are miscible in the full composition range. Likewise, the ion-ion interactions in ILs have a large orientational dependence [18], which leads to ILs+MSs mixtures with complex structuring at the nanoscopic level [19,20], with macroscopic properties not predictable using simple mixing rules [17,21], and thus with complex structure-property relationships [22,23,24,25].

The application of ILs+MSs has been considered in many technologies such as reaction media [26], electrolytes for batteries [27], polymerization [28], enzymatic processes [29], CO2 capture [30], cellulose solvents [31] or interfacial phenomena-related applications [32]. Likewise, ILs+MSs mixtures have been proposed to decrease solvents volatility, and thus to control hazards and toxicity of industrial solvents [33]. Another relevant application stands on the use of ILs as entrainers for azeotropic distillation [34], for example for systems

involving complex intermolecular forces such as ethanol + water mixtures [35] in which the understanding of the involved IL / MSs intermolecular forces can provide the required tools for designing suitable IL entrainers. Despite of the technological interest on ILs+MSs mixtures, studies on the behaviour of these mixed fluids at the microscopic level are still scarce, which hinders to obtain relationships between molecular level features and macroscopic physicochemical properties. This is of a great relevance considering the large number of possible ILs, which combined with MSs and considering the suitability of developing ILs+MSs mixtures in the full composition range for many systems, leads to many possible mixtures which cannot be considered only from experimental approaches. Therefore, a systematic approach should be considered in which the main types of ILs and MSs are studied to infer the main characteristics of intermolecular forces as a function of the considered ions and functional groups in MSs and their effect on the structuring of mixed systems in the liquid state.

The available studies on ILs+MSs have considered several types of prototypical MSs such as acetone [36], acetonitrile [37] or dimethyl sulfoxide [38]. Regarding possible MSs for developing ILs+MSs mixtures, 1-alkanol is of great relevance as well [39,40]. The study of self-association in 1-alkanols by hydrogen bonding (homoassociation), the development of ion-alkanol hydrogen bonding (heteroassociation) and its effect on anion-cation interactions (hydrogen bonding and coulombic forces) and on ion-clustering, and the evolution the evolution of all these forces upon mixing with ILs in the full composition range leads to pivotal information on the evolution of different types of hydrogen bonding upon mixing [19]. This complex balance of intermolecular forces in ILs+alkanol solutions may lead even to micro- or mesoscopically heterogeneous mixtures [41,42]. Therefore, 1-butyl-3-methylimidazolium bis(trifluoromethylsulfonyl)imide ([BMIM][Tf_2N]) + ethanol (EtOH), Fig. 1, binary mixtures were studied in this work using a combined experimental and theoretical approach for contributing to the development of the knowledge database for ILs+MSs properties. [BMIM][Tf_2N] ILs was selected because both anion and cation can develop hydrogen bonding, and thus EtOH molecules could develop hydrogen bonding with both ions. This possibility was checked in this work and its effect on anion-cation interactions were also analysed. Likewise, [BMIM][Tf_2N] is a moderately viscous fluid (51.0 mPa s at 298.15 K and 0.1 MPa) [43], which is a clear advantage when comparing with other ILs. Our group reported a theoretical study using molecular dynamics (MD) simulations on

[BMIM][Tf_2N]) + EtOH mixtures and some physicochemical properties are available in the literature elsewhere [44], where non-ideal behaviour with EtOH molecules developing hydrogen bonding with [Tf_2N] anion but with anion-cation interaction through CH(2) site maintained in the full composition range were studied. In this work, the characteristic of short range interactions in [BMIM][Tf_2N] + EtOH mixtures were theoretically analysed by using density functional theory (DFT) of molecular cluster, allowing to calculate the most suitable interaction sites according to interaction energies and topology. Likewise, dynamic viscosity and refraction index were measured in the full composition range because of the relationship of these properties with intermolecular forces. Spectroscopical studies using Raman IR were also carried out for a wide range of mixture concentrations to infer experimentally the mechanism of interactions and the evolution of hydrogen bonding. The reported results combined with previous studies lead to a full characterization of the studied system as a model of imidazolium-based ILs + primary alcohol mixtures.

2. Methods

DFT calculations were carried out with Gaussian 09 [45] software for B3LYP [46,47] /6-31+G(d,p) theoretical level. Previous literature studies have showed that B3LYP functional allowed a reasonably accurate description of intermolecular interactions of ILs [48,49,50,51] and ILs + MSs mixtures [52,53], including those involving alkanols [54]. Different types of molecular clusters were considered and optimized at the reported theoretical level. IR spectra were calculated and attention was paid to vibrations corresponding to functional groups which could be involved in hydrogen bonds. Interaction energies were calculated according to the following equations:

$$\Delta E_1 = E_{multimer} - \sum_i E_{i,monomers} \quad (1)$$

$$\Delta E_2 = \Delta E_1 - \Delta E_{1,[\mathrm{BMIM}][\mathrm{Tf2N}]} \quad (2)$$

$$\Delta \nu_1 = \nu_1 - \nu_{1,[\mathrm{BMIM}]^+} \quad (3)$$

$$\Delta \nu_2 = \nu_2 - \nu_{2,\mathrm{EtOH}} \quad (4)$$

where $E_{multimer}$ stands for the counterpoise corrected energy of studied clusters (cation / anion ionic pairs or cation / anion / EtOH), $E_{i,monomers}$ for the energy of each *I* monomer

involved in the corresponding cluster, $\Delta E_{1,[BMIM][Tf2N]}$ for the interaction energy in cation / anion ionic pair, ν_1 for the stretching vibrational frequency of C-H(2) bond in imidazolium ring and ν_2 for the stretching vibrational frequency of O-H bond in EtOH (in multimers), $\nu_{1,[BMIM]+}$ for ν_1 in isolated $[BMIM]^+$ cation and $\nu_{2,EtOH}$ for ν_2 in isolated EtOH. The analysis of intermolecular interactions through quantum theory of Atoms in a Molecule (Bader's theory [55], AIM) and Reduced Density Gradient methods (RDG) [56] was carried out with Multiwfn program [57].

Regarding samples used for experimental measurements, [BMIM][Tf_2N] was synthesized and characterized as previously reported [58] whereas commercial EtOH (Sigma-Aldrich, 99.8 % purity) was used for all the measurements. [BMIM][Tf_2N] + EtOH mixtures were prepared gravimetrically with a Mettler AT 261 balance (±1 10^{-5} g). Water content was determined before measurements with Karl Fischer coulometric titration (Metrohm 831 KF coulometer, 0.1 g samples, ±0.3%), Table S1 (Supplementary Material).

Dynamics viscosities, η, were measured in the 293 to 323 K range, at 1 bar and in the full composition range using an electromagnetic VINCI Tech. EV1000 viscometer. The experimental procedure for viscosity calibration and measurements was described in detail in a previous work [59] leading to an uncertainty for the reported dynamic viscosity data of ±2%. Refraction indices, n_D, were measured for the sodium D-line using a Leica AR600 thermostated refractometer (±0.01 K) to ±5 10^{-5} [60]. Raman IR study was carried out with a WITEC Alpha300R confocal Raman microscope operating at ambient temperature (20 ± 1 °C) with laser excitation at 531.92 nm. Procedures were validated by comparison of experimental properties obtained in this work for pure solvents with literature values showing excellent agreement, Table S2 (Supplementary Information).

3. Results and discussion

Analysis of [BMIM][Tf_2N] – EtOH Interaction Using DFT. Considering that the subject of this study is the analysis of [BMIM][Tf_2N] – EtOH interactions, first we will analyze the characteristics of hydrogen bonding in both independent systems, i.e. interactions between EtOH molecules and anion-cation interactions in [BMIM][Tf_2N]. The characteristics of ethanol self-aggregation by hydrogen bonding in liquid state are well-known, showing interaction through hydroxyl groups with a separation of donor-acceptor separation of 2.8 Å and 1.8 hydrogen bonds per molecule [61]. The characteristics of EtOH-EtOH hydrogen

bonding has been also studied in the literature using quantum chemistry methods. Three different major conformers can be considered for EtOH monomers (defined according to the C-C-O-H dihedral): a trans and two gauche conformations [62], with trans conformer being the most stable although the energy difference between these three conformers is as low as 0.119 kcal mol^{-1} [63]. Theoretical studies on EtOH dimmers have led to conflicting results, whereas some authors have proposed that trans-trans was the most stable dimmer [64] other studies have considered gauche-gauche as the most stable one [65]; nevertheless, the difference between both types of interaction is lower than 2 kJ mol^{-1}. Results in Fig. 2 show the trans-trans EtOH dimmer calculated in this work, the donor-acceptor distance and the counterpoise corrected interaction energy agrees with previous literature results [64,65]. The formation of trans-trans dimer reported in Fig. 1 leads to an increase of O-H bond distance, r_2 in Fig. 1, specially for OH group acting as hydrogen bond donor, Table 1. This EtOH-EtOH interaction leads to large redshifting of the vibrational frequencies of stretching vibrations of OH group acting as hydrogen bond donor and almost negligible changes for the acceptor OH group, Table 2.

The properties of [BMIM] - [Tf_2N] interaction were analyzed in the following step. The conformational equilibrium of [Tf_2N] anion has been studied in the literature [66], with two conformers, c_1 and c_2 (Fig. 3), present at equilibrium because of the small energy difference between them (~ 3.5 kJ mol^{-1}, with c_2 being the lowest energy conformer). This is reproduced by results in Fig. 3 at the considered theoretical level. Regarding the [BMIM] - [Tf_2N] ionic pairs, the interaction of c_1 and c_2 [Tf_2N] conformers with [BMIM] cation through CH(2) site (Figs. 4a and 4b) and through CH(1) sites (Fig. 4c and 4d) were considered. Previous literature studies have showed that [Tf_2N] anion interacts preferently through [BMIM] CH(2) position [67,68,69], which is confirmed by results reported in Fig. 4. Energy differences between ionic pairs interacting through CH(2) and CH(1) sites are large enough to consider that this IL will develop hydrogen bonding through CH(2) site. The lowest energy interacting pair correspond to the one in which [Tf_2N] anion in c_2 conformer interacts with cation through CH(2) site, Fig. 4b, whereas the energy difference regarding to the pair corresponding to c_1 conformer at cation CH(2) is larger than RT at 298.15 K, Fig. 4a, which should lead to a preference for the interaction according to mechanism reported in Fig. 4b [70,71]. [Tf_2N] in the c_2 conformer allows a stronger hydrogen bonding through CH(2) imidazolium site because donor – acceptor distances are lower, Figs. 4a and 4b. Likewise,

hydrogen bonding through imidazolium CH(1) sites has larger donor – acceptor distances, i.e. weaker interactions are produced, Figs. 4c and 4d. Therefore, anion-cation interaction through CH(2) imidazolium site leads to large interaction energy, enlargement of C-H(2) bond distance (r_1) in comparison with isolated cation, and a large redshifting of C-H(2) stretching frequency (ν_1), Table 1. Larger anion-clusters were considered containing two cations and two anions, with anions in c_1 or c_2 conformers, Fig. 5. Results for the lowest energy conformers are reported in Fig. 5 for cation-anion-cation-anion linear clusters show that the configuration containing both anions in c_1 conformer, Fig. 5a, leads to lower energies than the one containing both anions in c_2 conformer, Fig. 5b. Comparison of results in Figs. 5 and 4 show that the formation of larger anion-cation clusters leads to an enlargement of donor-acceptor distances for hydrogen bonding through imidazolium CH(2) site, but this effect is more remarkable for c_2 conformer, which would justify its larger energy. Likewise, results in Fig. 5 show that anion-cation interactions through the imidazolium CH(1) site can be developed through the anion oxygen atoms allowing effective interaction of anion with one neighbor cation through the CH(2) site and with the other one though the CH(1) site.

The DFT analysis of [BMIM] - [Tf_2N] – EtOH complexes was carried out considering anion-cation interacting through CH(2) site, Fig. 6, or through CH(1) site, Fig. 7 (although with lower interaction energies, in absolute value, than those for interactions through CH(2) site), and thus the possible interaction sites for EtOH were studied for each arrangement. Regarding cluster containing anion-cation pairs interacting through CH(2) site (with lower energies than those through CH(1) site), seven lowest energy configurations were obtained, Fig. 6, which main properties are reported in Table 2. These configurations lead to large interaction energies (ΔE_1) in the order #7 > #3 > #2 > #1 > #4~#5 >#6. This ordering shows that configurations with EtOH interacting with oxygen atoms in [Tf_2N] anion (#7, #3, #2 and #1) lead to larger interaction energies than those with the EtOH interacting with the imidazolium cation through the CH(1) site (#4, #5 and #6), in agreement with larger EtOH contributions to the total interaction energy (ΔE_2), Table 1. This agrees with previous results showing the trend of EtOH molecules to develop hydrogen bonding with [Tf_2N] in liquid phase [59]. Likewise, EtOH – [Tf_2N] interaction leads to large redshifting of EtOH OH stretching frequency (ν_2), whereas small redshifting are obtained for ν_2 redshifting when interacting with cation CH(1) site. Likewise, the development of ion-EtOH interactions leads

to changes in anion-cation hydrogen bonding through CH(2) site, as confirmed by the larger donor-acceptor distance (d_1), shorter C-H(2) bonds (r_1) and smaller redshifting for ν_1, in comparison with ionic pair in absence of EtOH, Table 2. Therefore, interaction with EtOH leads to a weakening of anion-cation interactions, which is balanced by the contribution rising from anion-EtOH hydrogen bonding. Results in Table 2 also show that the strength of anion-EtOH hydrogen bonding (ΔE_2) are in the range or larger than those for EtOH-EtOH interactions (Table 2 and Fig. 2), and thus, in liquid [BMIM] – [Tf_2N] – EtOH the development of anion-EtOH interactions would be superior than that of EtOH-EtOH hydrogen bonding, i.e. disrupting EtOH hydrogen bonding network upon mixing. Regarding the interaction of EtOH molecules with ionic pairs interacting through cation CH(1) site, results in Fig. 7 show that EtOH-cation hydrogen bonding through CH(2) site (#8 and #9, Fig. 7) leads to similar interaction energies of those structures with EtOH interacting with cation through CH(1) sites (#4, #5 and #6 in Fig. 6 and Table 2). Likewise, anion-EtOH interaction can be also developed effectively when anion is hydrogen bonded to cation in CH(1) site leading to structures with slightly lower interaction energies than those when anion is hydrogen bonded with cation through CH(2) site (#11 in Fig. 7 compared with #7 in Fig. 6 and Table 2.

AIM and RDG analysis of [BMIM] – [Tf_2N] – EtOH interaction is reported in Fig. 8 for the lowest energy conformer (#7 in Fig. 6 and Table 2). The topological properties of the interactions in [BMIM] – [Tf_2N] – EtOH cluster are characterized by the presence of several bond critical points (BCPs, type (3,-1) according to Bader's [55]) and ring critical points (RCPs, [55]), Fig. 8a. Anion-cation hydrogen bonding through CH(2) site is characterized by a BCP (blue dot #1 in Fig. 8a) between CH(2) hydrogen atom and nitrogen atom in the anion, but closer to the hydrogen atom. The definition of hydrogen bonding according to AIM theory stands that electron density, ρ, and laplacian of electron density, $\nabla^2\rho$, must be in the range 0.002 to 0.04 a.u. and 0.020 to 0.139 a.u, respectively [72], and thus values for BCP #1 show that anion-cation hydrogen bonding is in the middle range of strength according to AIM theory even with the presence of one EtOH molecule hydrogen bonded to the anion, i.e. the weakening mentioned in previous paragraphs upon interaction with EtOH is not large and most of the properties of anion-cation interaction through CH(2) site are maintained. Likewise, anion-cation interaction is also characterized by the presence of BCPs (blue dots #2 and #3, Fig. 8a) between the hydrogen atoms of the alkylimidazolium chains close to the ring and nitrogen atoms in the cation, and although ρ and $\nabla^2\rho$ for these BCPs are lower than

those for BCP #1 they are inside the AIM range for defining hydrogen bonds. The EtOH – anion interaction through the anion oxygen atom is also characterized by a BPC (blue dot #4 in Fig. 8a) with ρ and $\nabla^2\rho$ larger than those for BCP #1, showing strong EtOH – anion hydrogen bonding. Likewise, the presence of additional BCPs and several RCPs both in the space around anion-cation hydrogen bonding in CH(2) site and around the EtOH-anion hydrogen bonding, Fig. 8a, show additional intermolecular interactions contributing to the stabilization of the clusters, which although weaker than the mentioned hydrogen bonds would lead to efficient global interactions in liquid state. Regarding the RDG analysis reported in Fig. 8b shows that the intermolecular regions corresponding to the possible hydrogen bonds leads to RDG spots indicating moderately strong hydrogen bonds (light blue areas) whereas additional spots corresponding to strong van der Waals interactions (green areas) are obtained in other intermolecular regions showing additional contributions to the total interaction energy.

Thermophysical Properties. Results in previous section analysed using DFT methods the properties of intermolecular interactions considering small sized clusters because of computational restrictions, thus obtaining a picture of forces acting on short range. Nevertheless, additional features are present in bulk liquids phase in which medium and long-range effects must be considered together with steric effects not considered in gas phase calculations. Selected experimental properties were measured in the full composition range are discussed in this section.

Several authors have experimented the physicochemical properties of [BMIM][Tf_2N] + EtOH mixtures. Heintz et al. [73] and measured the activity coefficient at infinite dilution of EtOH in [BMIM][Tf_2N] leading to a value of 1.88 at 298.15 K, in agreement with strong solute-solvent interactions. Andreatta et al. [44] measured density, viscosity and refractive index of [BMIM][Tf_2N] + EtOH at 298.15 K in the full composition range, showing negative excess volume (with minima for EtOH rich mixtures) and negative deviations from linearity for viscosity (with minima for equimolar mixtures). Experimental properties obtained in this work are reported in Tables S3 and S4 (Supplementary Information). Experimental dynamic viscosity data were fitted to Vogel-Fulcher-Tamman equation, with fitting parameters reported in Table S5 (Supplementary Information). Results obtained in this work for dynamic viscosity are in excellent agreement with the results that were reported by Andreatta et al.

at 298.15 K [44], Fig. 9. The composition and temperature dependence of the studied properties is reported in Fig. 10. Refraction index, n_D, follows a non-linear evolution with increasing [BMIM][Tf_2N] molar fraction, x, showing a steeped increase up to x~0.2 and then a small linear increase up to pure IL. This behavior leads to positive deviations of linearity, Δn_D, with maxima at x~0.2 for all the studied temperatures, Fig. 10a. These results are justified considering that negative excess volume (with minima at x~0.2 [44]) points to less available free volume than in ideal mixtures [74,75], which leads to larger n_D than from linear evolution from composition, i.e. positive Δn_D with maxima at the same mixture composition than excess volume minima. Therefore, results in Fig. 10a reporting the effects of the addition of the studied IL to EtOH show that although having a disruptive effect amongst the EtOH, intermolecular forces leads to highly efficient molecular packing. Regarding these volumetric effects, they are relevant up to x~0.2 from which IL dominated fluids are formed and thus linear evolution of n_D is inferred. The free volume origin of the behavior of n_D with mixture composition is confirmed by the increase of Δn_D with increasing temperature.

Viscosity behavior is very different than that of excess volume and refraction index. The viscosity of both neat fluids is very different and viscosity increases in a non-linear way with increasing IL mole fraction leading to negative mixing dynamic viscosity, $\Delta\eta$, in the whole composition range for all the studied isotherms with the observed minima around x~0.6, Fig. 10b. These results are analyzed considering that the evolution of viscosity with mixture composition should depend on free volume effects, on the size and shape of the diffusing molecules and on the strength of intermolecular forces. For IL rich mixtures, EtOH molecules would disrupt large ionic clusters, i.e. decreasing viscosity, and at the same time they would develop hydrogen bonds with anions, but negative mixing dynamic viscosity shows the prevailing disrupting role of EtOH molecules. Therefore, disrupting effect of EtOH molecules on ILs interactions would control mixtures viscosities for IL-rich solutions. Regarding, EtOH rich mixtures, results in Fig. 10b show that although the size of IL cluster would increase with increase IL mole fraction, the moderate viscosity increase up to roughly equimolar mixtures points to small IL cluster solvated by EtOH molecules hydrogen bonded between them. The decrease, in absolute value, of $\Delta\eta$ with increasing temperature, but maintaining the mixture composition for the minima, shows weaker intermolecular forces

with increasing temperature, leading to smaller molecular clusters diffusing in a medium with lower free volume, i.e. viscosities closer to linear behavior with composition.

Intermolecular Forces from Raman Spectroscopy. Raman IR spectra provides direct proofs of intermolecular forces in bulk liquid phases. The Raman spectra for [BMIM][Tf_2N] + EtOH mixtures is complex, and thus the analysis was carried out selecting relevant spectral regions considering the most relevant functional groups regarding intermolecular forces. Results in Fig. 11 show the behavior in the 3100 to 3300 cm^{-1} corresponding to the stretching vibrations of OH group in EtOH. Previous literature studies [76] have showed that this region corresponds in neat EtOH to four gaussian peaks assigned to (peak1) OH in ethanol monomers (3588 cm^{-1}), (peak2) OH involved in weak interactions with neighbor EtOH molecules (3474 cm^{-1}), (peak3) OH involved in a single hydrogen bond, acting as donor (3362 cm^{-1}), and (peak4) OH participating in two hydrogen bonds, i.e. OH groups acting as donor and acceptor (3244 cm^{-1}). The distribution of these peaks through peak deconvolution in pure EtOH would be 3.8, 20.7, 38.9 and 36.6 % for peaks1 to peak4, respectively [76]. Therefore, experimental Raman spectra were deconvoluted using Gaussian peaks, with linear baseline correction, for the 3100 to 3700 cm^{-1} range. The four peaks obtained were 3540, 3455, 3351 and 3244 cm^{-1} (for peak1 to peak4, respectively) in neat EtOH, corresponding to 7.0, 20.9, 48.7 and 23.4 % distribution percentages, which is in reasonable agreement with previous literature results [76], and shows a minor fraction of monomers with most of liquid EtOH corresponding to EtOH molecules involved in hydrogen bonding. The evolution of 3100 to 3700 cm^{-1} region with mixture composition shows remarkable changes with increasing IL concentration, Fig. 11. The most remarkable feature with increasing [BMIM][Tf_2N] is the increase of peak1 and the decrease of the peaks below 3500 cm^{-1} corresponding to hydrogen bonded EtOH molecules. The frequency of peak1 shifts from 3540 cm^{-1} in neat EtOH to 3573 cm^{-1} for [BMIM][Tf_2N] 2.29 M solutions. For [BMIM][Tf_2N] concentrations larger than 2.5 M it was not possible to deconvolute peaks and a single peak at 3573 cm^{-1} with a shoulder at lower frequencies was inferred. The evolution with [BMIM][Tf_2N] concentration of the percentage area of the four peaks in the 3100 to 3700 cm^{-1} region is reported in Fig. 12. These results show the vanishing of peak IV for concentrations larger than 1.5 M but the population of EtOH participating in two hydrogen bonds is still relevant for lower concentrations. Peak 3 also decreases with increasing IL

concentration but showing relevant population for concentrations lower than 2.0 M. The additional relevant features in Fig. 12 are the increase of peak 1 and peak 2 with increasing IL concentration showing that for concentrations larger than 2.0 M these two features lead to 98 % of the total peak area. Therefore, these results show that the addition of the studied IL decreases the degree of association of EtOH, which evolve toward monomers or molecules developing single hydrogen bonds. The increase of peak II can be attributed to EtOH molecules hydrogen bonded to ions. Two additional spectral regions were considered in the analysis, Fig. 13. The 2800 to 3100 cm^{-1} region corresponds to stretching vibrations of C-H groups in imidazolium rings (CH(2) and CH(1)), peaks above and below 3000 cm^{-1} [77], and to vibrations of EtOH C-H groups, which appear at lower frequencies, Fig. 13a. Regarding the peaks corresponding to imidazolium CH groups, they do not show any shifting with increasing IL concentration, and thus, the interaction of EtOH with [BMIM] cation should be discarded. Results in Fig. 13b corresponds to spectra in the 1000 to 130 cm^{-1}, which contains relevant vibrational features of [Tf_2N] anion. The peak at 1245 cm^{-1} corresponds to the symmetric stretching of CF_3, and its frequency does not change when the IL is mixed with EtOH, i.e. EtOH molecules are not hydrogen bonded to this functional group in the anion. The peaks in the 1040 to 1080 cm^{-1} correspond to symmetric stretching vibrations of the SO group in [Tf_2N] and to the CO group in EtOH (at lower frequency), peaks corresponding to SO group suffer a weak shifting and thus the interaction of EtOH with this functional group is also weak. This agrees with the evolution of EtOH association reported in Fig. 12, which show increasing population of monomers and weakly bonded molecules, and thus, confirming that the main role of the studied IL on EtOH structuring is disruption through the decrease of EtOH hydrogen bonding by increasing the population of monomers and molecules weakly bonded to the anion in the IL.

4. Conclusions

Intermolecular forces in 1-butyl-3-methylimidazolium Bis(trifluoromethylsulfonyl)imide + ethanol mixtures were studied using a combination of quantum chemistry, thermophysical and Raman spectroscopy studies. The reported results showed that these binary mixtures are characterized by the disruptive effect of the studied ionic liquid on ethanol structure, which leads to an increase in the monomers population with increasing ionic liquid concentration. Although ethanol can develop hydrogen bonds with both cation and anion as

the theoretical results show, the large trend to develop cation-anion interactions seems to hinder ethanol-ion hydrogen bonding, which is limited to weak ethanol-anion ones. Only for ionic liquid concentrations lower than 1.5-2 M ethanol are remarkably self-hydrogen bonded both in dimmers or larger associates. This justifies the large deviations from ideality of these mixtures, which is most relevant for ionic liquid mole fractions lower than 0.2-0.3.

Acknowledgement

This work was funded by Junta de Castilla y León (Spain, project BU324U14). The statements made herein are solely the responsibility of the authors.

Electronic Supplementary Information

Table S1 (water contents of used samples); Table S2 (comparison of thermophysical data with literature); Table S3 (experimental refractive index data); Table S4 (experimental dynamic viscosity data); Table S5 (Vogel-Fulcher-Tamman coefficients for viscosity).

Table 1

Selected relevant properties for isolated $[BMIM]^+$, isolated EtOH, $[BMIM]^+$ / $[Tf_2N]^-$ ionic pair (Fig. 4) an $[BMIM]^+$ / $[Tf_2N]^-$ / EtOH (Fig. 5) clusters, obtained from optimizations at B3LYP / 6-31+G(d,p) theoretical level. Distances (r_1, r_2 and d_1) and vibrational frequencies (ν_1 and ν_2) are defined according to Fig. 1; the remaining properties are defined according to eqs. (1-4)

system	r_1 / Å	r_2 / Å	d_1 / Å	$-\Delta E_1$ /	$-\Delta E_2$	ν_1 / cm^{-1}	ν_2 / cm^{-1}	$\Delta\nu_1$ / cm^{-1}	$\Delta\nu_2$ / cm^{-1}
$[BMIM]^+$ [a]	1.0794	–	–	–	–	3298.63	–	0	–
EtOH [b]	–	0.9654	–	–	–	–	3835.19	–	0
EtOH dimer [c]	–	0.9742 [f] 0.9661 [g]	–	–	–	–	3665.29 [f] 3833.41 [g]	–	-169.90 [f] -1.78 [g]
$[BMIM]^+$ / $[Tf_2N]^-$ [d]	1.0927	–	2.101	302.16	0	3098.97	–	-199.66	–
$[BMIM]^+$ / $[Tf_2N]^-$ / EtOH [e]									
1	1.0906	0.9726	2.148	322.91	20.75	3131.53	3710.10	-167.10	-125.09
2	1.0870	0.9733	2.208	326.01	23.85	3181.21	3697.64	-117.42	-137.55
3	1.0870	0.9742	2.205	333.96	31.80	3177.12	3676.01	-121.51	-159.18
4	1.0873	0.9661	2.167	319.57	17.41	3164.41	3829.91	-134.22	-5.28
5	1.0908	0.9664	2.105	319.92	17.76	3123.56	3826.84	-175.07	-8.35
6	1.0902	0.9664	2.139	316.79	14.63	3140.41	3825.52	-158.22	-9.67
7	1.0876	0.9748	2.072	336.16	34.00	3159.33	3665.03	-139.30	-170.16

Properties calculated for: [a] isolated $[BMIM]^+$, [b] isolated EtOH, [c] EtOH dimer reported in Fig. 2; [d] $[BMIM]^+$ / $[Tf_2N]^-$ ionic pair reported in Fig. 4a; [e] $[BMIM]^+$ / $[Tf_2N]^-$ / EtOH clusters reported in Fig. 6; [f] OH acting as hydrogen bond donor; [g] OH acting (only) as hydrogen bond acceptor

Figure Captions.

Fig. 1. Molecules studied in this work together with labelling for relevant distances (r_1, r_2 and d_1) and stretching vibrational frequencies (ν_1 and ν_2).

Fig. 2 Geometry of EtOH dimer from optimization at B3LYP / 6-31+G(d,p) theoretical level. *ΔE* shows counterpoise corrected interaction energy.

Fig. 3. Geometries of C_1 and C_2 conformers of $[Tf_2N]^-$ obtained from optimizations of isolated anions at B3LYP / 6-31+G(d,p) theoretical level. *ΔE* shows counterpoise corrected energy difference between both conformers (C_1 conformer more stable).

Fig. 4. Geometries of $[BMIM]^+$ / $[Tf_2N]^-$ ionic pairs obtained from optimizations of isolated pairs at B3LYP / 6-31+G(d,p) theoretical level. *ΔE* shows counterpoise corrected energy difference with reference to interacting pair in panel b. The four reported conformations show interactions through (a,b) CH(2) and (c,d) CH(1) position of the imidazolium ring in the cation for (a,c) C_1 and (b,d) C_2 conformers of $[Tf_2N]$.

Fig. 5. Geometries of $[BMIM]^+$ / $[Tf_2N]^-$ / $[BMIM]^+$ / $[Tf_2N]^-$ cluster calculated at B3LYP / 6-31+G(d,p) theoretical level. *ΔE* shows counterpoise corrected energy difference with reference to interacting pair in panel a.

Fig. 6. Geometries of $[BMIM]^+$ / $[Tf_2N]^-$ ionic pairs interacting with EtOH molecules calculated at B3LYP / 6-31+G(d,p) theoretical level. All structures with $[BMIM]^+$ / $[Tf_2N]^-$ interactions through CH(2) site.

Fig. 7. Geometries of $[BMIM]^+$ / $[Tf_2N]^-$ ionic pairs interacting with EtOH molecules calculated at B3LYP / 6-31+G(d,p) theoretical level. All structures with $[BMIM]^+$ / $[Tf_2N]^-$ interactions through CH(1) site.

Fig. 8 (a) AIM and (b) RDG analysis of $[BMIM]^+$ / $[Tf_2N]^-$ / EtOH cluster (structure #7 in Fig. 6). In panel a, (blue dots) (3,-1) BCPs and (red dots) (3,+1) RCPs. Intermolecular bond paths are omitted in panel a for the sake of visibility.

Fig. 9. Comparison of experimental dynamic viscosity, η, and mixing dynamic viscosity, $\Delta\eta$, for x [BMIM][Tf_2N] + (1-x) EtOH mixtures at 298.15 K obtained in this work (black symbols) and from Andreatta et al. [44] (empty symbols). Lines show polynomial (η) or Redlich-Kister ($\Delta\eta$) fittings for guiding purposes.

Fig. 10. (a) Refraction indices, n_D, and deviations from linearity in refractive indices, Δn_D, (b) dynamic viscosity, η, and mixing dynamic viscosity, $\Delta\eta$, in x [BMIM][Tf_2N] + (1-x) EtOH mixtures at several temperatures. Points show experimental data and lines polynomial (for n_d and η) or Redlich-Kister (for Δn_d and $\Delta\eta$) fittings for guiding purposes.

Fig. 11. Raman spectra in the 3100 to 3700 cm^{-1} region for [BMIM][Tf_2N] + EtOH mixtures as a function of [BMIM][Tf_2N] molar concentration, c, at ambient temperature (~22 ^oC). Panel (a) shows experimental results and panels (b) to (g) show deconvolution using gaussian profiles (dashed lines) and the sum of these gaussian profiles (red curves).

Fig. 12. Percentage contribution to the total area, % *area*, for peaks reported in Fig. 11. Peaks I to IV are numbered according to increasing wavenumber.

Fig. 13. Raman spectra in selected frequency ranges for [BMIM][Tf_2N] + EtOH mixtures as a function of [BMIM][Tf_2N] molar concentration, c, at ambient temperature (~22 ^oC).

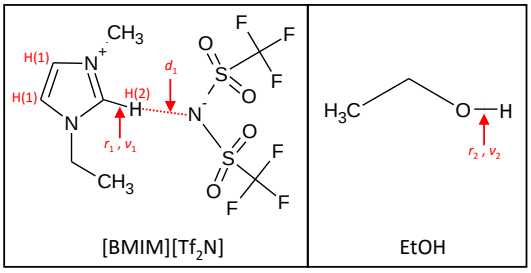

Fig. 1.

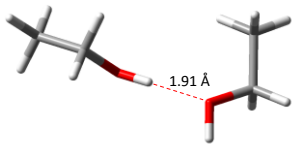

$\Delta E = E_{dimer} - 2E_{monomer}$ =-20.91 kJ mol^{-1}

Fig. 2

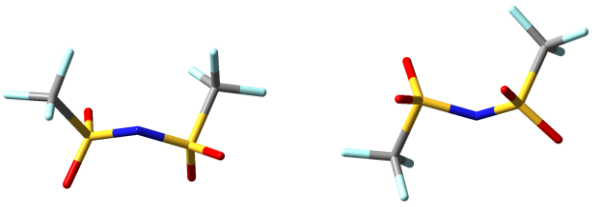

C_1 C_2

$$\Delta E = E_{C1} - E_{C2} = -1.84 \text{ kJ mol}^{-1}$$

Fig. 3.

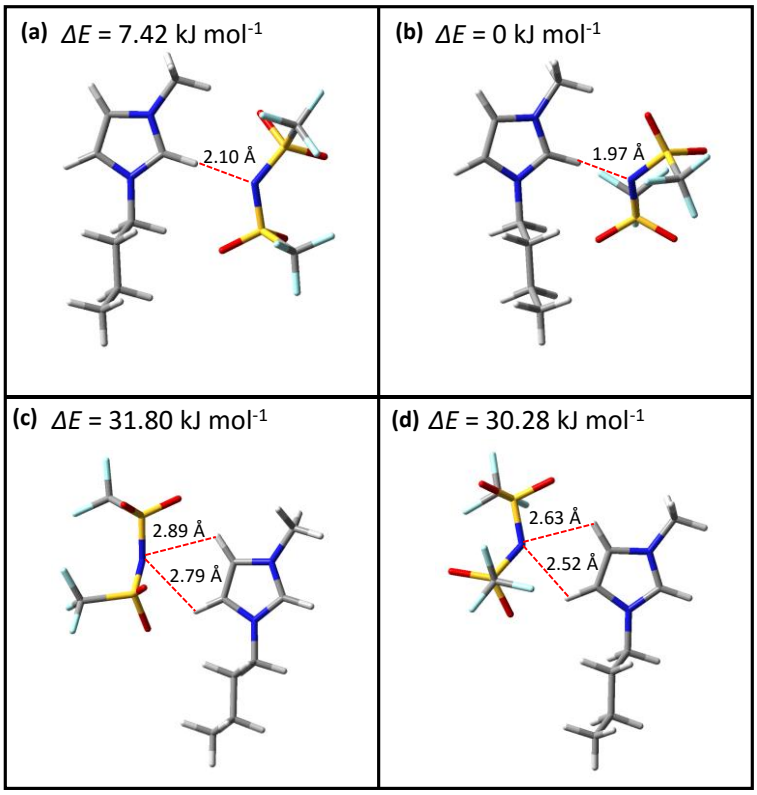

Fig. 4.

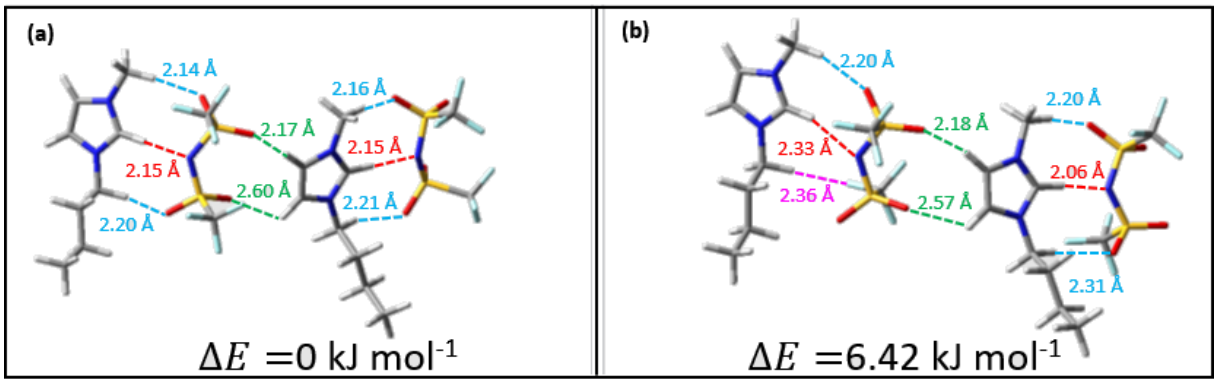

Fig. 5.

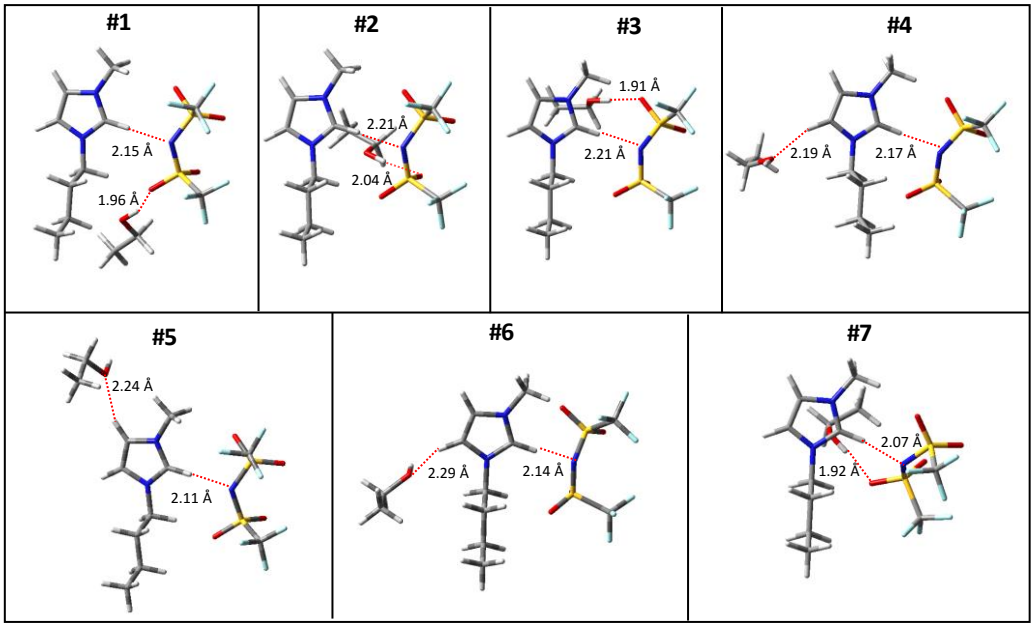

Fig. 6.

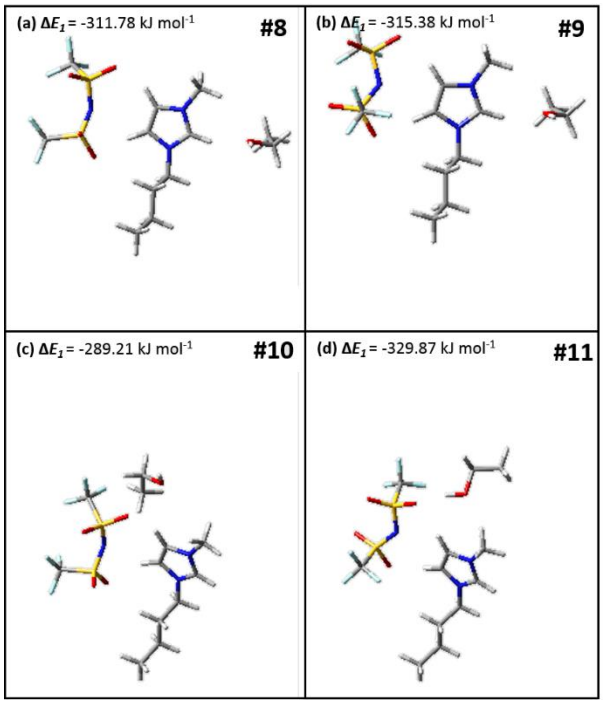

Fig. 7.

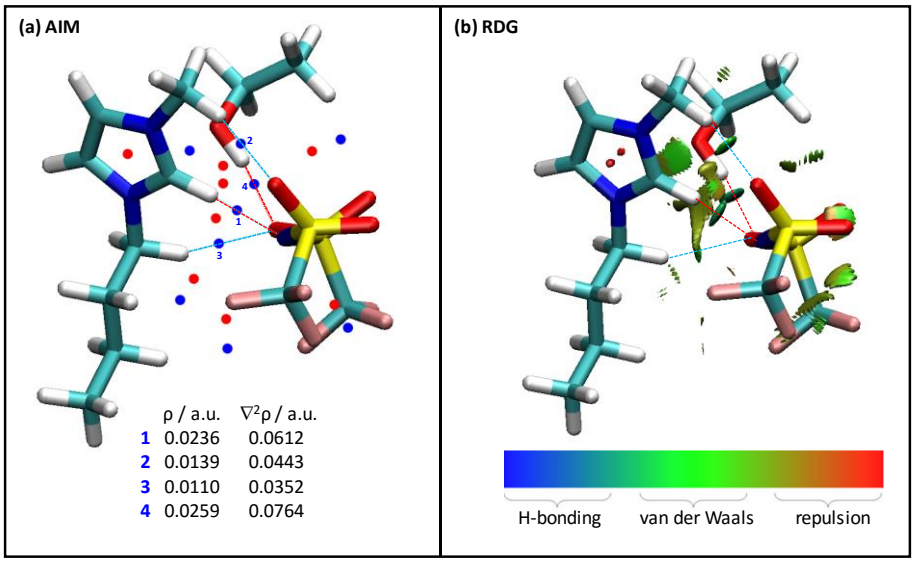

Fig. 8.

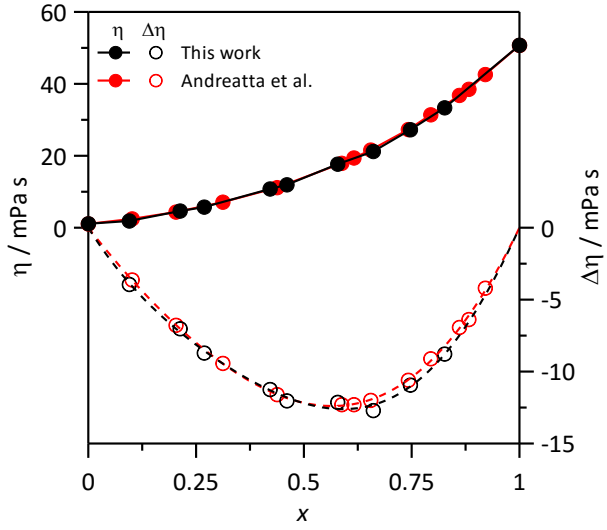

Fig. 9.

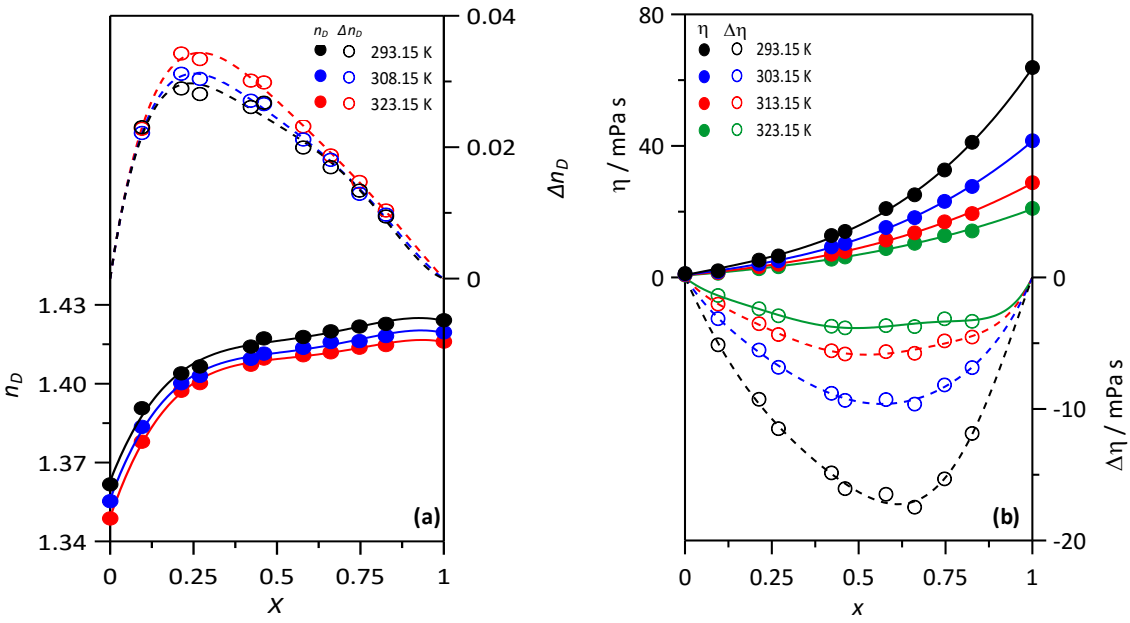

Fig. 10.

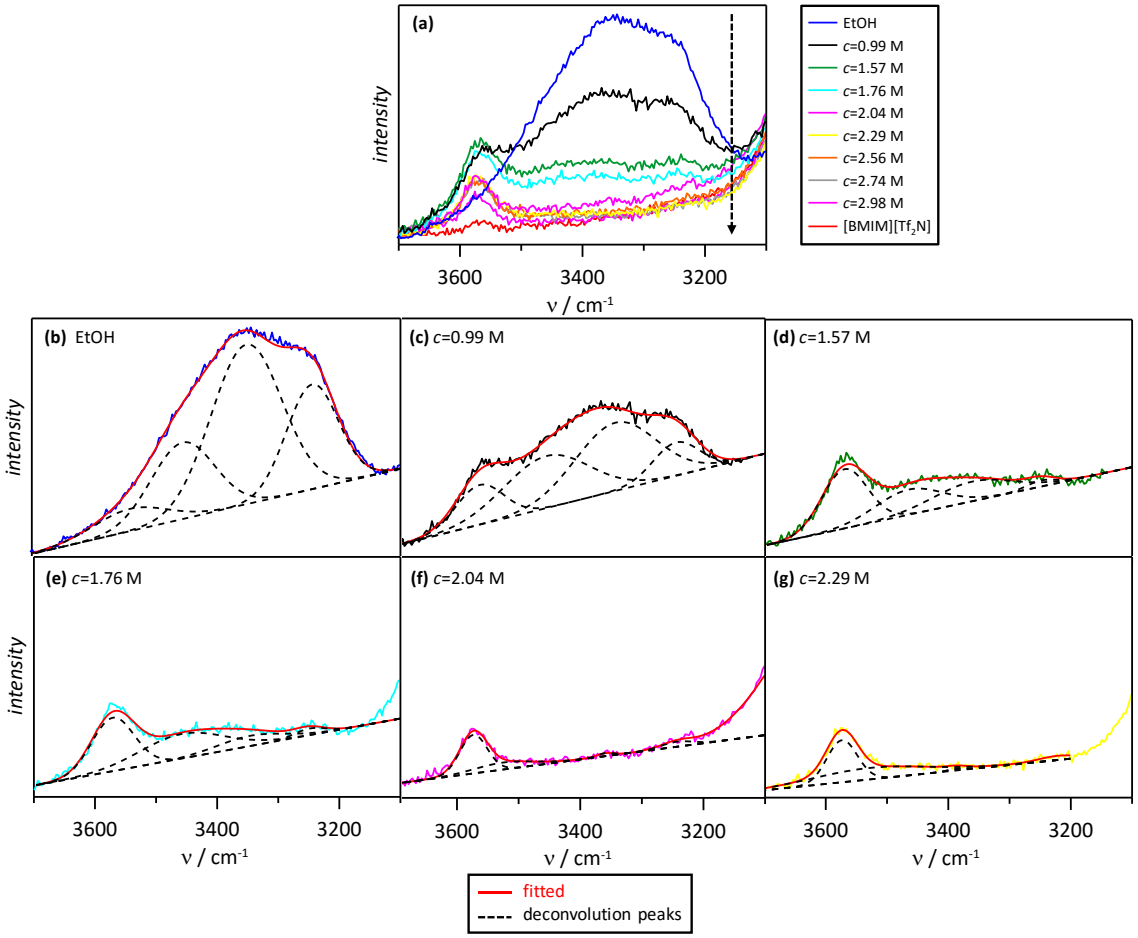

Fig. 11.

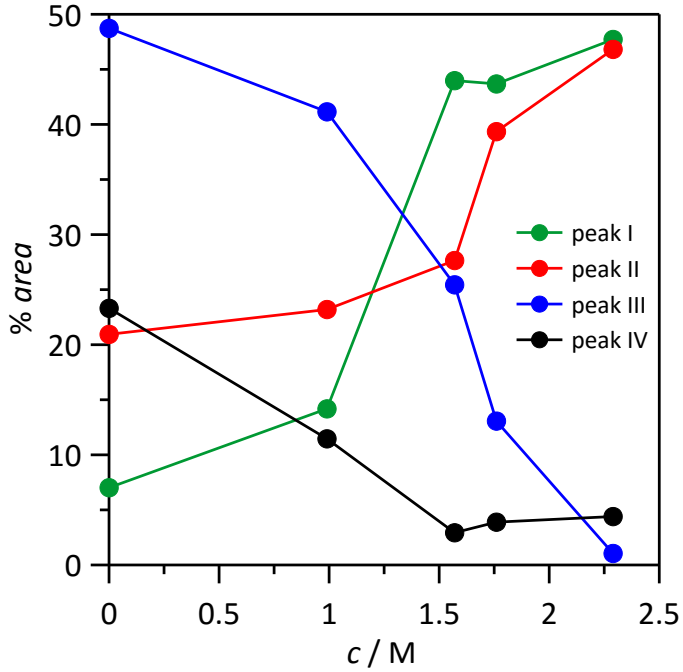

Fig. 12

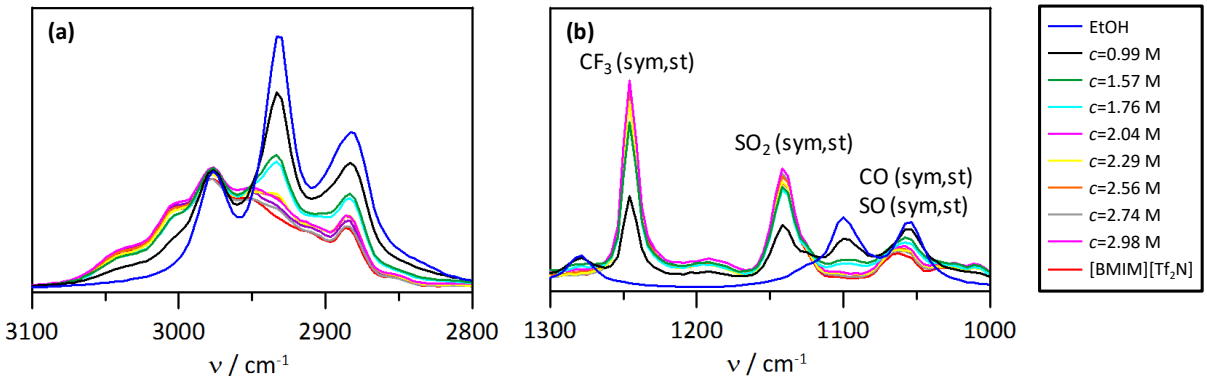

Fig. 13

References

[1] Y. Kohno, H. Ohno, H. Chem. Comm. 48 (2012) 7119-7130.
[2] E. T. Fox, E. Paillard, O. Borodin, W. A. Henderson, J. Phys. Chem. C 117 (2013) 78-84.
[3] Y. Huang, Y. Zhao, S. Zeng, X. Zhang, S. Zhang, Ind. Eng. Chem. Res. 53 (2014) 15270-15277.
[4] K. Noack, A. Leipertz, J. Kiefer, J. Mol. Struct. 1018 (2012) 45-53.
[5] B. Docampo-Alvarez, V. Gomez-Gonzalez, T. Mendez-Morales, J. Carrete, J. R. Rodriguez, O. Cabeza, L. J. Gallego, L. M. Varela, J. Chem. Phys. 140 (2014) 214502.
[6] L. M. Varela, T. Mendez-Morales, J. Carrete, V. Gomez-Gonzalez, B. Docampo-Alvarez, L. J. Gallego, O. Cabeza, O. Russina, J. Mol. Liq. 210 (2015) 178-188.
[7] N. C. Osti, K.L. van Aken, M. W. Thompson, F. Tiet, D. Jiang, P. T. Cummings, Y. Gogotsi, E. Mamontov, J. Phys. Chem. Lett. 8 (2017)167-171.
[8] B. A. Marekha, K. Sonoda, T. Uchida, T. Tokuda, A. Idrissi, T. Takamuku, J. Mol. Liq. 232 (2017) 431-439.
[9] A. M. Smith, A. A. Lee, S. Perkin, Phys. Rev. Lett. 118 (2017) 096002.
[10] S. W.Coles, A. M. Smith, M. V. Fedorov, F. Hausen, S. Perkin, Faraday Discuss. 206 (2018) 427-442.
[11] A. B. McEwen, H. L. Ngo, K. LeCompte, J. L. Goldman, J. Electrochem. Soc. 146, (1999) 1687-1695.
[12] Y. Zhu, S. Murali, M. D. Stoller, K. Ganesh, W. Cai, P. J. Ferreira, A. Pirkle, R. M. Wallace, K. A. Cychosz, M. Thommes, D. Su, E. A. Stach, R. S. Ruoff, Science 332 (2011) 1537-1541.
[13] X. Yang, C. Cheng, Y. Wang, L. Qiu, D. Li, Science 341 (2013) 534-537.
[14] V. V. Chaban, Phys. Chem. Chem. Phys. 17 (2015) 31839-31849.
[15] O. Ciocirlan, O. Croitoru, O. Iulian, J. Chem. Thermodyn. 101 (2016) 285-292.
[16] F. Yang, Q. Ma, X. Wang, Z. Liu, J. Chem. Eng. Data 62 (2017) 1628-1638.
[17] D. R. MacFarlane, A. L. Chong, M. Forsyth, M. Kar, R. Vijayaraghavan, A. Somers, J. M. Pringle, Faraday Discuss. (2017) DOI: 10.1039/C7FD00189D
[18] R. Hayes, G. G. Warr, R. Atkin, Chem. Rev. 115 (2015) 6357-6426.
[19] G. Shrivastav, A. Gupta, A. Rastogi, D. Dhabal, H. K. Kashyap, J. Chem. Phys. 146 (20178) 064503.
[20] T. Shimomura, D. Kodama, M. Kanakubo, S. Tsuzuki, J. Phys. Chem. B 121 (2017) 2873-2881.
[21] H. K. Stassen, R. Ludwig, A. Wulf, J. Dupont, Chem. Eur. J. 21 (2015) 8324–8335.
[22] M. Chen, R. Pendrill, G.Windmalm, J. W. Brady, J. Wohlert, J. Chem. Theory Comput. 10 (2014) 4465-4479.
[23] Y. Huang, Y. Zhao, S. Zheng, X. Zhang, s. Zhang, Ind. Eng. Chem. Res. 53 (2014) 15270-15277.
[24] M. Lashkarbolloki, J. Thermophys Heat Tr. (2017) DOI: 10.2514/1.T5153
[25] S. Atashrouz, H. Mirshekar, A. Hemmati-Sarapardeh, M. Keshavarz-Moraveji, B. Nasernejad, Korean J. Chem. Eng. 34 (2017) 425-439.
[26] S. T. Keaveney, T. L. Greaves, D. F. Kennedy, J. B. Harper, J. Phys. Chem. B 120 (2016) 12687-12699.
[27] A. Khan, C. Zhao, Electrochem. Comm. 49 (2014) 1-4.
[28] S. Dewilde, J. Winters, W. Dehaen, K. Binnemans, Macromolecules 50 (2017) 3089-3100.
[29] M. de Graca-Nascimento, J. M. Ramos-da Silva, J. C. da Silva, M. Miranda-Alves, J. Mol. Catal. B Enzym. 112 (2015) 1-8.
[30] J. J. Fillion, J. E. Bennett, J. F. Brennecke, J. Chem. Eng. Data 62 (2017) 608-622.
[31] S. Napso, D. M. Rein, R. Khalfin, Y. Cohen, J. Polym. Sci., Part B: Polym. Phys. 55 (2017) 888–894.
[32] M. Jitvisate, J. R. T. Seddon, J. Phys. Chem. C 121 (2017) 18593-18597.
[33] V. V. Chaban, P. V. Prezhdo, J. Phys. Chem. Lett. 2 (2011) 2499-2503.
[34] A. B. Pereiro, J. M. M. Araujo, J. M. S. S. Esperanca, I. M. Marrucho, L. P. N. Rebelo, J. Chem. Thermodyn. 46 (2012) 2-28.
[35] N. Gjineci, E. Boli, A. Tzani, A. Detsi, E. Voutsas, Fluid Phase Equilibr. 424 (2016) 1-7.
[36] E. Ruiz, V. R. Ferro, J. Palomar, J. Ortega, J. J. Rodriguez, J. Phys. Chem. B 117 (2013) 7388-7398.
[37] M. Liang, Mx. X. Zhang, A. Kaint, N. P. Ernsting, M. Maroncelli, J. Phys. Chem. B 118 (2014) 1340-1352.
[38] J. C. Jiang, K. H. Lin, S. C. Li, P. M. Shih, K. C. Hung, S. H. Lin, H. C. Chang, J. Chem. Phys. 134 (2011) 044506.
[39] E. J. Gonzalez, P. F. Requejo, A. Dominguez, E. A. Macedo, J. Sol. Chem. 42 (2013) 746-763.
[40] E. Vercher, F. J. Llopis, v. González-Alfaro, P. J. Miguel, V. Orchillés, A. Martínez-Andreu, J. Chem. Thermodyn. 90 (2015) 174-184.
[41] W. Schroer, A. Triolo, O. Russina, J. Phys. Chem. B 120 (2016) 2638-2643.
[42] O. Russina, A. Sferrazza, R. Caminiti, A. Triolo, J. Phys. Chem. Lett 5 (2014) 1738-1742.
[43] K. R. Harris, M. Kanakubo, L. A. Woolf, J. Chem. Eng. Data 52 (2007) 1080-1085.

[44] A. E. Andreatta, A. Arce, E. Rodil, A. Soto, J. Sol. Chem. 39 (2010) 371-383.
[45] K. E. Riley, M. Pitoňák, P. Jurečka, P. Hobza, M. J. Frisch, G. W. Trucks, H. B. Schlegel, G. E. Scuseria, M. A. Robb, J. R. Cheeseman, G. Scalmani, V. Barone, B. Mennucci, G. A. Petersson, H. Nakatsuji, M. Caricato, X. Li, H. P. Hratchian, A. F. Izmaylov, J. Bloino, G. Zheng, J. L. Sonnenberg, M. Hada, M. Ehara, K. Toyota, R. Fukuda, J. Hasegawa, M. Ishida, T. Nakajima, Y. Honda, O. Kitao, H. Nakai, T. Vreven, J. A. MontgomeryJr., J. E. Peralta, F. Ogliaro, M. Bearpark, J. J. Heyd, E. Brothers, K. N. Kudin, V. N. Staroverov, T. Keith, R. Kobayashi, J. Normand, K. Raghavachari, A. Rendell, J. C. Burant, S. S. Iyengar, J. Tomasi, M. Cossi, N. Rega, J. M. Millam, M. Klene, J. E. Knox, J. B. Cross, V. Bakken, C. Adamo, J. Jaramillo, R. Gomperts, R. E. Stratmann, O. Yazyev, A. J. Austin, R. Cammi, C. Pomelli, J. W. Ochterski, R. L. Martin, K. Morokuma, V. G. Zakrzewski, G. A. Voth, P. Salvador, J. J. Dannenberg, S. Dapprich, A. D. Daniels, O. Farkas, J. B. Foresman, J. V. Ortiz, J. Cioslowski, and D. J. Fox, Gaussian 09, Revision C.01, Gaussian, Inc., Wallingford CT, 2010.
[46] A.D. Becke, J. Chem. Phys. 98 (1993) 5648–5652.
[47] C. T. Lee, W. T. Yang, R. G. Parr, Phys Rev B 37 (1988) 785–789.
[48] E. I. Izgorodina, U. L. Bernard, D. R. MacFarlane, J. Phys. Chem. A 113 (2009) 7064-7072.
[49] S. Grimme, W. Hujo, B. Kirchner, Phys. Chem. Chem. Phys. 14 (2012) 4878-4883.
[50] S. Zahn, D. R. MacFarlane, E. I. Izgorodina, Phys. Chem. Chem. Phys. 15 (2013) 13664-13675.
[51] A. Knorr, R. Ludwig, Scintific Reports 5 (2015) 17505.
[52] Z. Song, H. Wang, L. Xing, J. Sol. Chem. 38 (2009) 1139-1154.
[53] I. Bahadur, M. I. K. Momin, N. A. Koorbanally, M. Sattari, E. E. Ebenso, L. M. Katata-Seru, S. Singh, D. Ramjugernath, J. Mol. Liq. 213 (2016) 13-16.
[54] H. Li, P. Zhou, J. Zhang, D. Li, X. Li, X. Gao, J. Mol. Liq. 251 (2018) 51-60.
[55] R. F. W. Bader, Atoms in Molecules—A Quantum Theory; Oxford University Press: Oxford, 1990.
[56] E. R. Johnson, S. Keinan, P. Mori-Sánchez, J. Contreras-García, A. J. Cohen, W. Yang, J. Am. Chem. Soc. 132 (2010) 6498-6506.
[57] T. Lu, F. Chen, J. Comput. Chem. 33 (2012) 580-592.
[58] M. Atilhan, J. Jacquemin, D. Rooney, M. Khraisheh, S. Aparicio, Ind. Eng. Chem. Res. 52 (2013) 16774-16785.
[59] R. Alcalde, G. García, M. Atilhan, S. Aparicio, Ind. Eng. Chem. Res. 54 (2015) 10918-10924.
[60] B. García, R. Alcalde, S. Aparicio, J. M. Leal, Phys. Chem. Chem. Phys. 4 (2002) 5833-5840.
[61] A. H. Narten, J. Chem. Phys. 80 (1984) 3387-3391.
[62] S. M. Mejia, J. F. Espinal, A. Restrepo, F. Mondragón, J. Phys. Chem. A 111 (2007) 8250-8256.
[63] R. K. Kakar, C. R. Quade, J. Chem. Phys. 72 (1980) 4300-4307.
[64] L. González, O. Mó, M. Yánez, J. Chem. Phys. 111 (1999) 3855-3861.
[65] V.Dyczmons, J. Phys. Chem. A 108 (2004) 2080-2086.
[66] K. Fujii, T. Fujimori, T. Takamuku, R. Kanzaki, Y. Umebayashi, S. Ishiguro, J. Phys. Chem. B 110 (2006) 8179-8183.
[67] Y. U. Paulechka, G. J. Kabo, A. V. Blokhin, O. A. Vydrov, J. W. Magee, M. Frenkel, J. Chem. Eng. Data 48 (2003) 457-462.
[68] E. A. Turner, C. C. Pye, R. D. Singer, J. Phys. Chem. A 107 (2003) 2277-2288.
[69] S. A. Katsuba, E. E. Zvereva, A. Vidis, P. J. Dyson, J. Phys. Chem. A 111 (2007) 352-370.
[70] A. V. Blokhin, Y. U. Paulechka, A. A. Strechan, G. J. Kabo, J. Phys. Chem. B 112 (2008) 4357-4364.
[71] N. R. Dhumal, K. Noack, J. Kiefer, H. J. Kim, J. P`hys. Chem. A 118 (2014) 2547-2557.
[72] H. Roohi, A. R. Nowroozi, E. Anjomshoa, Comput. Theor. Chem. 965 (2011) 211–220.
[73] A. Heintz, L. M. Cásas, I. A. Nesterov, V. E. Emel'yanenko, S. P. Verevkin, J. Chem. Eng. Data 50 (2005) 1510-1514.
[74] P. Brocos, A. Piñeiro, R. Bravo, A. Amigo, Phys. Chem. Chem. Phys. 5 (2003) 550-557.
[75] M. Anouti, A. Vigeant, J. Jacquemin, C. Brigouleix, D. Lemordant, J. Chem. Thermodyn. 42 (2010) 834-845.
[76] J. Kiefer, F. Toni, K. E. Wirth, J. Raman Spectrosc. 46 (2015) 1124-1128.
[77] K. Noack, P. S. Schulz, N. Paape, J. Kiefer, Phys. Chem. Chem. Phys. 12 (2010) 14153-14161.